

# The photodissociation dynamics of nitric acid studied at 193 nm by LIF and REMPI–TOF methods

Qiang Li, Robert T. Carter, J. Robert Huber\*

*Physikalisch-Chemisches Institut der Universität Zürich, Winterthurerstrasse 190, CH-8507 Zürich, Switzerland*

Received 10 November 2000; in final form 4 December 2000

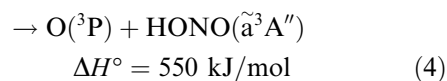
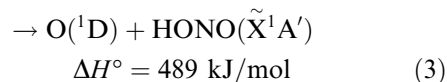
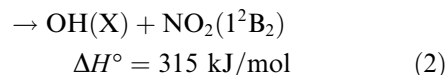
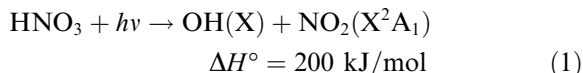
## Abstract

The 193 nm photodissociation of  $\text{HNO}_3$  in a supersonic jet has been investigated by LIF and REMPI–TOF techniques probing the  $\text{OH}(X^2\Pi)$  and the  $\text{O}(^3\text{P})$  products, respectively. The measured rotational state distribution of OH is shown to be dominated by a bimodal distribution consistent with the previously reported bimodal translational energy distribution of OH. An additional decay channel, yielding  $\text{O}(^3\text{P})$  fragments with high kinetic energy, has been observed and tentatively assigned to  $\text{HNO}_3 + h\nu \rightarrow \text{O}(^3\text{P}) + \text{HONO}(X^1A')$ . Energetic considerations indicate that about one third of the HONO products are unstable, decaying further to  $\text{OH} + \text{NO}$ . © 2001 Elsevier Science B.V. All rights reserved.

## 1. Introduction

Since photolysis of nitric acid  $\text{HNO}_3$  is an important source of OH radicals and  $\text{NO}_2$  in the stratosphere [1,2], the photodissociation of  $\text{HNO}_3$  has been extensively investigated in the laboratory under bulk and beam conditions [3–12]. The absorption spectrum of nitric acid exhibits a broad and structureless absorption with maxima at  $\sim 260$  nm due to a  $\pi^* \rightarrow n$  transition (absorption cross-section  $\sigma \approx 1.9 \times 10^{-20}$  cm<sup>2</sup>) and  $\sim 190$  nm due to a  $\pi^* \rightarrow \pi$  transition ( $\sigma \approx 1.6 \times 10^{-17}$  cm<sup>2</sup>) where both transitions are localized on the  $\text{NO}_2$  group [13]. Following photolysis at about 260 nm, the major primary process leads to the production of  $\text{OH} + \text{NO}_2$  [3,4]. LIF measurements on the nascent OH fragments [5–8] show no vibrational excitation

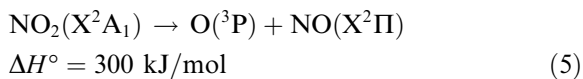
and a Boltzmann distribution among the rotational levels with  $E_{\text{rot}} \sim 5\%$  of the available energy  $E_{\text{avl}}$ . Using excitation at 193 nm a rich photochemistry becomes apparent including the following dissociation reactions, with their respective  $\Delta H^\circ$  values (taken as dissociation energies) [14]:



where the  $\text{NO}_2$  products of channel (1), in contrast to those of channel (2), have sufficient internal energy to undergo secondary dissociation

\*Corresponding author. Fax: +41-1-635-6838.

E-mail address: jrhuber@pci.unizh.ch (J.R. Huber).



The three major decay channels (1)–(3) have been studied by photofragment translational spectroscopy (PTS) [9] where the  $\text{NO}_2$  product of channel (2) was initially suggested to emerge more probably in the ground than in the electronic excited state. Using the same technique Myers et al. [10] have recently found an additional, minor pathway (4) and have assigned the channel (2) products to  $\text{OH}(\text{X})$  and  $\text{NO}_2(1^2\text{B}_2)$  using symmetry arguments in conjunction with correlation diagrams.

The reported branching ratios between the  $\text{NO}_2$  and HONO formations yielded conflicting results. Thus the quantum yield for channel (1) and (2) was reported by Turnipseed et al. [3] to be  $0.33 \pm 0.06$ , using LIF detection of the OH products, by Schiffman et al. [4] to be  $0.47 \pm 0.06$ , applying high resolution infrared absorption spectroscopy, and by Felder et al. [9] to be  $0.6 \pm 0.1$ , as estimated from PTS measurements. Myers et al. [10] carefully reinvestigated in their PTS study the efficiency of the various decay pathways and found a quantum yield for  $\text{NO}_2$  production of  $0.33 \pm 0.04$  and a branching ratio  $(\text{OH} + \text{NO}_2)/(\text{O} + \text{HONO}) = 0.50 \pm 0.05$ .

The OH fragments generated by photodissociation of nitric acid at 193 nm (or 212.5 nm) are exclusively in the vibrational ground state [7,11,12]. The LIF probing of the OH products has shown rotational state populations up to  $N'' \sim 20$ . However, the reported distributions, all obtained in the bulk phase, differ considerably. It appears that collisional deactivation prior to state probing has influenced some measurements. To resolve the discrepancies and thus to gain further information on channel (1) and (2) we carried out LIF measurements on nascent OH in a supersonic jet. This was paralleled by resonance enhanced multiphoton ionization time-of-flight (REMPI–TOF) measurements on oxygen fragments with the aim to assess possible OH formation from secondary dissociation of HONO. In the course of these investigations an additional decay process was revealed and tentatively assigned to



A fraction of the  $\text{HONO}(\tilde{\text{X}}^1\text{A}')$  products is shown to possess enough internal energy to decay to  $\text{OH} + \text{NO}$ . The present communication reports these results.

## 2. Experiment

The experimental set-up used in the present LIF work has been described in detail elsewhere [15,16]. A pulsed molecular beam of  $\text{HNO}_3$  seeded in He was generated with a specially designed corrosion-resistant valve driven by a piezoelectric translator [17]. Fuming nitric acid with a purity  $>99.5\%$  (Merck) was degassed to remove air and traces of  $\text{NO}_2$  until it was completely colorless. A gas mixture was formed by following He carrier gas with a stagnation pressure of 1–2.5 bar through a liquid sample of  $\text{HNO}_3$ . A mixture of 3%  $\text{HNO}_3$  in He was expanded through a pinhole aperture ( $d=0.5 \text{ mm}$ ) attached to the piezoelectric pulsed valve.

The photolysis at 193 nm was performed with an ArF excimer laser (Lambda Physik EMG 101 MSC). The softly focussed laser beam crossed the molecular beam at right angles 60 mm downstream from the nozzle. A counterpropagating probe laser beam recorded the nascent OH photofragments in the  $\text{A}^2\Sigma^+ \leftarrow \text{X}^2\Pi$  system (vibrational bands with  $\Delta v = 0$ ) [18,19] by LIF. The probe laser (Lambda Physik dye laser FL2002) had a linewidth of  $0.4 \text{ cm}^{-1}$  between 306 and 311 nm and was pumped by an XeCl excimer laser (Lambda Physik LPX200) operated with Sulforhodamine B dye and a frequency doubling crystal. Fluorescence from the OH fragments was collected at right angles to the plane of the molecular and laser beams by a Hamamatsu R928 photomultiplier tube. The signal was fed to a digital boxcar integrator (Stanford Research SR 250). Photodiodes monitored the photolysis and probe laser intensities to correct for shot to shot fluctuations. The OH signal produced by photodissociation grew linearly with the laser power in

the range of 3–16 mJ/cm<sup>2</sup>. A fluence of 5 mJ/cm<sup>2</sup> was therefore used to avoid multiphoton processes in dissociation. The probe laser fluence was kept below 0.1 mJ/cm<sup>2</sup> to avoid saturation effects. The linewidth measurements required the probe laser to be operated with an intracavity etalon providing  $\Delta\nu = 0.08 \pm 0.01$  cm<sup>-1</sup>.

The REMPI–TOF experimental set-up has been described previously [20,21]. The probe laser ran on Coumarin 47 yielding a pulse energy of 100–400  $\mu$ J at 225.6 nm following frequency doubling with a BBO crystal. The O(<sup>3</sup>P<sub>2</sub>) photofragment was detected by 2 + 1 REMPI at 225.60 nm via the 3p<sup>3</sup>P<sub>2</sub>–2p<sup>3</sup>P<sub>2</sub> transition [22]. The linearly polarized light of the photolysis laser at 193 nm was generated by passing the ArF excimer laser beam through a stack of 10 quartz plates at Brewster's angle, resulting in a polarization degree of 92%. The photodissociation experiments were carried out with parallel ( $\chi = 0^\circ$ ), perpendicular  $\chi = 90^\circ$ , and magic angle ( $\chi = 54.7^\circ$ ) polarizations relative to the detection axis. The photofragment speed distributions  $P(v)$  were obtained from the TOF data using a forward convolution method [23].

### 3. Results

#### 3.1. LIF measurements

A portion of the unpolarized LIF spectrum of OH(A<sup>2</sup> $\Sigma^+$  ← X<sup>2</sup> $\Pi$ ,  $\Delta v = 0$ ) fragments emerging from photodissociation of HNO<sub>3</sub> monomer at 193 nm is shown in Fig. 1. The rotational transitions in the 0–0 band of the A ← X transition were resolved and assigned according to Dieke and Crosswhite [18,19]. Consistent with published results [7,11,12] no signal was detected when the wavelength of the probe laser was tuned to the position of the OH (1,1) band indicating that the population of OH ( $v = 1$ ), and very probably also those of higher vibrational states, are negligible. Using standard procedures [24], the rotational state populations of the OH fragments, shown in Fig. 2a, were obtained from the LIF spectrum. The rotational distribution has a maximum at  $N'' = J'' \pm 1/2 = 1$  ( $N'' > 0$ ) followed by a continuous population decrease down to  $N'' = 18$ .

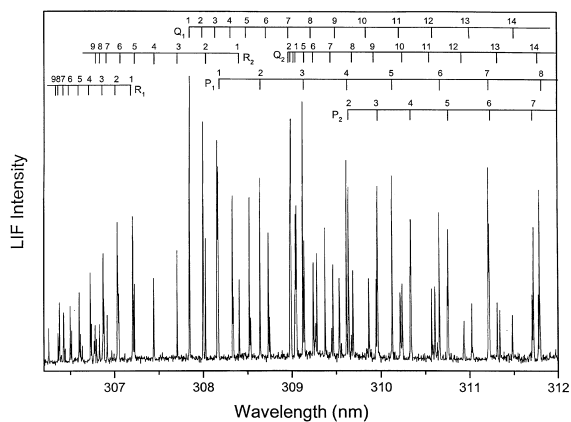


Fig. 1. Unpolarized LIF spectrum of nascent OH(A<sup>2</sup> $\Sigma^+$  ← X<sup>2</sup> $\Pi$ ) (0,0) following 193 nm photolysis of HNO<sub>3</sub> in a supersonic jet.

This distribution cannot be described by a single temperature, in contrast to the most recently reported results [12]. It is, however, similar to that reported by Schlütter and Kleinermanns [7], obtained in the bulk phase and at 212.5 nm. In view of the fact that the TOF spectrum of the OH product revealed a bimodal translational energy distribution [9,10], we partitioned the rotational state population into two distributions as shown in Fig. 2b. The high rotational excitation could be fitted by a Boltzmann distribution with a temperature  $T_r = 2500 \pm 150$  K, while that for the low excitation ( $N'' \leq 7$ ) cannot be approximated by a single temperature. The population ratio of the two distributions is roughly 2:1. This is similar to the ratio between the slow and the fast translational energy distributions of the OH fragments which have been assigned to reactions (2) and (1), respectively [9,10]. The mean rotational energy  $\langle E_{\text{rot}} \rangle = \sum_J P(J) E_{\text{rot}}(J)$ , where  $P(J)$  is the state distribution and  $E_{\text{rot}}$  the energy of a given rotational state, was found to be 1700 cm<sup>-1</sup> (20 kJ/mol) for the high and 120 cm<sup>-1</sup> (1.5 kJ/mol) for the low rotational state distribution.

Analysis of the spectrum further shows that the spin–orbit states  $\Pi_{3/2}$  and  $\Pi_{1/2}$  are equally populated within experimental errors for low and high  $J$ -states. From the intensities of the R and Q branches, we find the ratio of the lambda-doublet state populations to be  $\Pi(A')/\Pi(A'') = 1.3 \pm 0.1$ ,

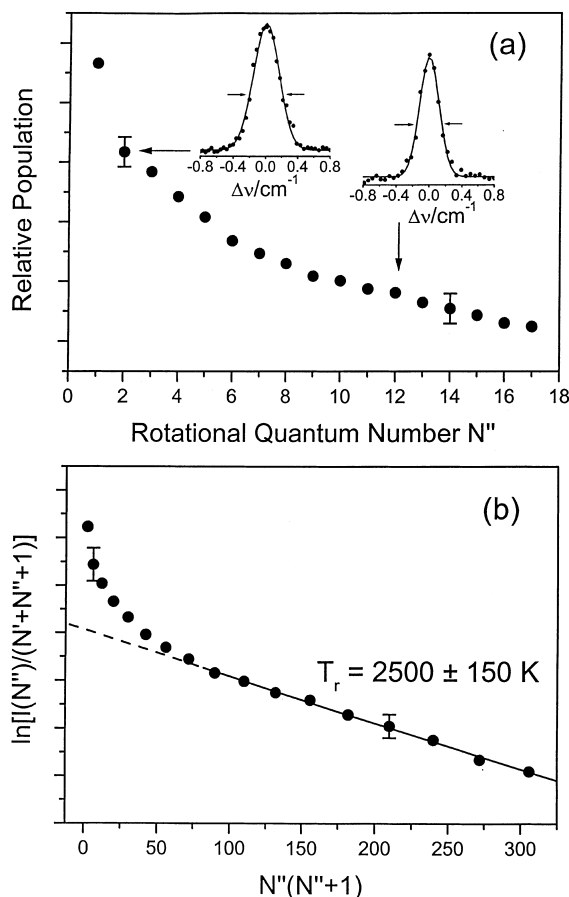


Fig. 2. (a) Data of the rotational state distributions of nascent  $\text{OH}(X^2\Pi, v=0)$  from photolysis of  $\text{HNO}_3$  at 193 nm. The inserts show the Doppler profiles for the  $P_1$  ( $N=2$ ) state (left) and the  $Q_1$  ( $N=12$ ) state (right). (b) Bimodal distribution analysis from the data in (a). Boltzmann plot fitted for  $N > 7$  and a superposed non-thermal distribution for  $N < 7$ .

indicating the symmetric state is preferred [25]. Also in this case no significant difference was found between the low and high  $J$ -states. Furthermore the translational energy of the OH fragment was estimated from the Doppler width of spectral lines shown in Fig. 2a. After deconvolution with the probe laser profile, a Doppler width of  $0.40 \pm 0.01 \text{ cm}^{-1}$  was measured for the  $P_1$  ( $N=2$ ) state which corresponds to a mean translational energy  $E_T(\text{OH}) = 7400 \text{ cm}^{-1}$  or 88 kJ/mol. On the other hand when the measurement was performed at  $Q_1$  ( $N=12$ ) a width of  $0.295 \pm 0.01 \text{ cm}^{-1}$  was found resulting in  $E_T(\text{OH}) =$

$4000 \text{ cm}^{-1}$  or 48 kJ/mol. This value agrees well with  $E_T(\text{OH}) = 49 \text{ kJ/mol}$  obtained in the PTS work [9] for the slow component of the OH fragments. The PTS result of the fast component was  $E_T(\text{OH}) = 116.5 \text{ kJ/mol}$  and is thus greater than our LIF value (88 kJ/mol). However this was expected because the LIF experiment at low  $J$ -states allowed a linewidth measurement only for the superimposed slow and fast components (cf. Fig. 2). Finally conservation of linear momentum provided the translational energy of the counter fragment  $\text{NO}_2$  which is 3600 and  $1500 \text{ cm}^{-1}$  (i.e. 43 and 18 kJ/mol) for the fast and slow components, respectively; the internal energy,  $E_{\text{int}}(\text{NO}_2) = E_{\text{avl}} - E_T(\text{OH}) - E_{\text{int}}(\text{OH}) - E_T(\text{NO}_2)$  is then 21 680 and  $27 900 \text{ cm}^{-1}$ , respectively. These findings are summarized in Table 1 and compared with previously reported results [7,12].

### 3.2. REMPI-TOF measurements

In order to assess possible other OH radical sources from  $\text{HNO}_3$  photolysis at 193 nm that may contribute to the OH rotational energy distributions of Fig. 2, we investigated dissociation reactions leading to HONO products with sufficient internal energy to undergo a unimolecular decay to  $\text{OH} + \text{NO}$ . Using the REMPI-TOF method we recorded the TOF profiles of the  $\text{O}(^3\text{P})$  fragments (in the strongest populated  $^3\text{P}_2$  spin-orbit state) which mirrors the internal energy distribution of the HONO counterfragments. Fig. 3 shows the experimental results taken at three polarization angles  $\chi$ . The profiles appear to consist of at least two velocity distributions. The analysis by a forward convolution procedure [23] yielded three speed distributions  $P(v)$  of  $\text{O}(^3\text{P})$  as depicted in Figs. 3 and 4a as dotted, dashed and chain-dashed curves. The main component (dotted line), representing  $\sim 50\%$  of all  $\text{O}(^3\text{P}_2)$  fragments, is centered at  $\bar{v} = 1100 \text{ m/s}$  and has an anisotropy parameter  $\beta = 0$ . This component can be assigned to the secondary dissociation (5) of the primary  $\text{NO}_2$  product of process (1) on the basis of the kinetic energy distribution of  $\text{NO}_2$  given by Felder et al. [9] and assuming a statistical unimolecular decay. The slower component (dashed line) with a mean speed of 700 m/s (accounting to  $\sim 20\%$ ) is attrib-

Table 1  
Photodissociation of HNO<sub>3</sub> at 193 nm (212.5 nm) in bulk phase [7,12] and in the molecular beam (energy in cm<sup>-1</sup>)

	Leu et al. [12] (193 nm)	Schlüter et al. [7] (212.5 nm)	This work (193 nm)	
			Fast component channel (2)	Slow component channel (1)
$E_{\text{avl}}$	35 570 <sup>a</sup>	30 400 <sup>a</sup>	35 100	35 100
$E_{\text{T}}(\text{OH})$	950 (2.7) <sup>b</sup>	930 (3)	120 (0.3)	1700 (4.8)
$E_{\text{T}}(\text{OH})$	2330 (6.6)	–	9700 <sup>c</sup> (27.6)	4000 (11.4)
$E_{\text{T}}(\text{NO}_2)$	860 (2.4)	–	3600 (10.3)	1500 (4.3)
$E_{\text{int}}(\text{NO}_2)$	31 430 (88.3)	–	21 680 (61.8)	27 900 (79.5)
$F_2(\Pi_{3/2})/F_1(\Pi_{1/2})$	1.1 ± 0.1	1.01 ± 0.09	1.0 ± 0.1	1.0 ± 0.1
$\Pi(A')/\Pi(A)''$	~1	1.82 ± 0.16	1.3 ± 0.1	1.3 ± 0.1

<sup>a</sup>  $E_{\text{avl}} = h\nu + E_{\text{int}}(\text{HNO}_3 \text{ at } 300 \text{ K}) - D_0(\text{HO}-\text{NO}_2)$ .

<sup>b</sup> The number in the parenthesis refers to % of the  $E_{\text{avl}}$ .

<sup>c</sup> Taken from the PTS results [9] since our LIF data represent a superposition of the two components.

uted to the primary O(<sup>3</sup>P) from reaction (4) since the  $E_{\text{T}}$  distribution, shown in Fig. 4b and described below, parallels that measured for this reaction by Myers et al. [10] with PTS. The fastest component (chain-dashed line in Figs. 3 and 4) with  $\bar{v} = 3500$  m/s (accounting to ~30%) had no equivalent in the literature. For the latter two components the analysis provided the same anisotropy with  $\beta = +0.9 \pm 0.1$ . It is noted that the estimated contributions of the three components are directly related to quantum yields only if the spin-orbit states of the O fragments are statistically populated.

The total translational energy distribution  $P(E_{\text{T}})$  was obtained from  $P(v)$  using the relationship  $P(E_{\text{T}}) = P(v)(dv/dE_{\text{T}})$  [21]. For each of the three components,  $P(E_{\text{T}})$  is reproduced in Fig. 4b. To identify the reaction giving rise to the distribution centered at  $E_{\text{T}}^{\text{tot}} \sim 140$  kJ/mol a dissociation process releasing O(<sup>3</sup>P) with a high recoil (3500 m/s) has to be considered. Suitable candidates are the photodissociation of the primary NO<sub>2</sub> products to O(<sup>3</sup>P) + NO(X), and reaction (6) leading to O(<sup>3</sup>P) + HONO(X), whereby both fragments are in their electronic ground states. In the first case the absorption of a photon also by nascent NO<sub>2</sub> would generate O(<sup>3</sup>P) fragments with a maximum translational energy  $E_{\text{T}}^{\text{max}} = E_{\text{avl}} = 2h\nu - D_0(\text{HO}-\text{NO}_2) - D_0(\text{NO}-\text{O}) = 740$  kJ/mol where  $2h\nu = 2 \times 619$  kJ/mol is the energy of the two absorbed photons,  $D_0(\text{HO}-\text{NO}_2) = 200$  kJ/mol and  $D_0(\text{NO}-\text{O}) = 300$  kJ/mol [14] are the respective dissociation energies, and

$E_{\text{int}}(\text{HNO}_3)$  has been neglected as HNO<sub>3</sub> is entrained in a supersonic jet. This  $E_{\text{T}}^{\text{max}}$  value corresponds to a maximum velocity of 7800 m/s which is much greater than the velocity found in the experiment given by the onset at ~4500 m/s in Fig. 4a. Thus this result and the extremely low absorption coefficient of NO<sub>2</sub> at 193 nm [26] make this secondary dissociation unlikely. Left with reaction (6), the maximum translational energy of this process is  $E_{\text{T}}^{\text{max}} = h\nu - D_0(\text{HONO}-\text{O}) - E_{\text{el}}(\text{HONO})$  with  $h\nu = 619$  kJ/mol and  $D_0(\text{HONO}-\text{O}) = 298$  kJ/mol [14]. In this equation we have included a possible electronic excitation ( $E_{\text{el}}$ ) of the HONO product. With HONO in the ground state  $E_{\text{T}}^{\text{max}} = E_{\text{avl}} = 320$  kJ/mol which exceeds the onset at ~230 kJ/mol (Fig. 4b) by 90 kJ/mol. For a polyatomic fragment this is not unusual and would indicate that even the fastest HONO product species possess an appreciable amount of internal energy. On the other hand an electronic excitation of HONO can clearly be excluded since the  $S_1(A^1A')$  or  $T_1(\tilde{a}^3A'')$  states would require 310 and 252 kJ/mol [27], respectively and hence would put  $E_{\text{T}}^{\text{max}}$  at 10 and 68 kJ/mol in contradiction to the experiment. We are therefore inclined to attribute the fast O(<sup>3</sup>P<sub>2</sub>) fragments measured in our experiment to reaction (6).

In returning to our initial goal of identifying OH sources, we determine the HONO fragments of reaction (6) which have sufficient energy to overcome the dissociation barrier ( $D_0(\text{HO}-\text{NO}) = 201$  kJ/mol [14]) to OH and NO. In Fig. 4b the threshold energy,  $E_{\text{T}}^{\text{thresh}} = E_{\text{avl}} -$

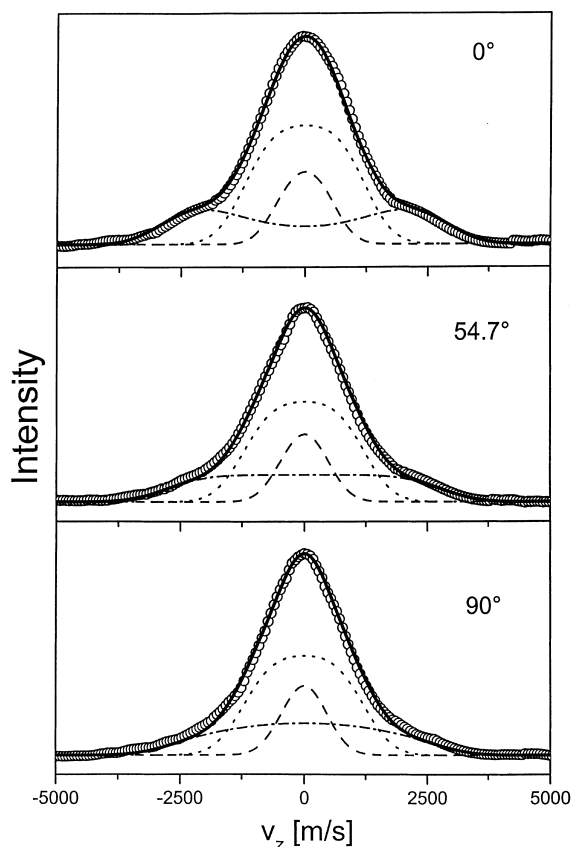


Fig. 3. REMPI-TOF data of the  $O(^3P_2)$  fragments from  $HNO_3$  photodissociation at 193 nm recorded under three different polarization angles. The open circles indicate the experimental data. The dotted line indicates channel (5), the dashed line channel (4) and the chain-dashed line channel (6). The corresponding photofragment speed distributions are given in Fig. 4a. The solid line is the sum of the three contributions.

$D_0(\text{HO}-\text{NO}) = 120 \text{ kJ/mol}$ , for this secondary dissociation marks the beginning of the region (dark shadowed) where HONO spontaneously decays. By comparing in Fig. 4a the areas under the TOF profiles of the spontaneous  $\text{NO}_2$  decay and of reaction (6) we obtain an estimate of the quantum yield of the latter. Assuming for both reactions a statistical spin-orbit population of the O fragments and a quantum yield of about 0.22 [10] for reaction (1) which provides the unstable  $\text{NO}_2$ , we find  $\phi \sim 0.11$  for reaction (6). Since only about one third of that gives rise to OH fragments, less than 10% of the total amount of OH frag-

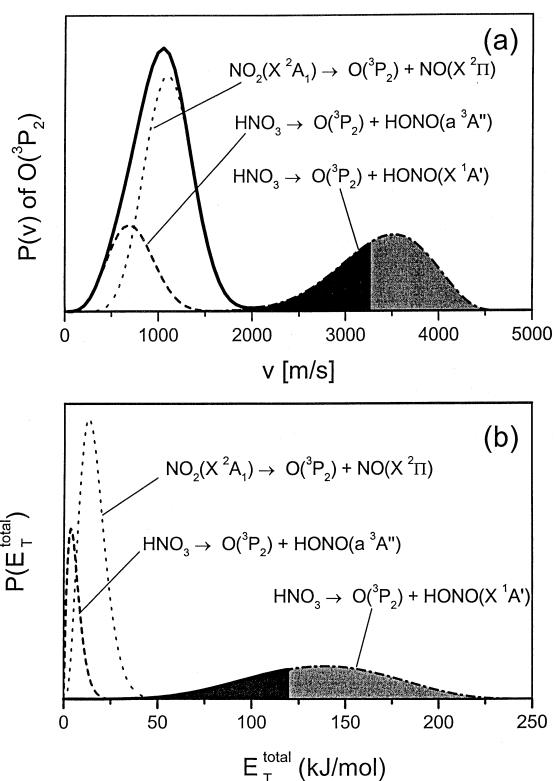


Fig. 4. (a)  $O(^3P_2)$  photofragment speed distribution determined for the 193 nm dissociation of  $HNO_3$ . In correspondence to Fig. 3 the dotted line refers to channel (5), the dashed line to (4) and the chain-dashed line to (6). The solid line shows the sum of (4) and (5). The dark shaded area in (a) and (b) marks the part for which HONO decays spontaneously. (b) Total translational energy distributions  $E_T^{\text{total}}$  of  $O(^3P)$  + counterfragment for channels (4)–(6) obtained by transformation of the speed data in (a).

ments created in reactions (1), (2) and (6) stem from reaction (6). A probably more reliable assessment of this yield is given below.

#### 4. Discussion and conclusion

Reaction channels (1) and (2) create OH radicals with different translational energy distributions [9,10]. It was therefore expected that the measured rotational state distribution (Fig. 2a) is not described by a single temperature in contrast to a recent claim by Leu et al. [12]. As shown in

Fig. 2b we approximated the data by two distributions, one described by a temperature of 2500 K and the other by a non-thermal low  $J$ -excitation. Based on the Doppler profile, i.e. kinetic energy measurements as well as their relative contributions, the non-thermal distribution can be assigned to the fast OH channel (2) with  $\text{NO}_2(1^2\text{B}_2)$ , the thermal distribution to channel (1) with  $\text{NO}_2$  in the ground state. Although this assignment is unambiguous the present analysis is only approximate since the small contribution of OH radicals from hot HONO emerging from channel (6) has been neglected. This additional contribution will introduce a small error to the rotational energies given in Table 1.

In our previous PTS measurements, where the aim was to characterize the main decay processes, no indication of the minor channel (4) was found, but later Myers et al. [10] provided evidence for this pathway. The present REMPI results on  $\text{O}(^3\text{P})$  (Fig. 4) corroborate their findings and are consistent with their assignment. In addition we found a new dissociation channel generating  $\text{O}(^3\text{P})$  fragments with high kinetic energies. According to the analysis given in the results section, the most likely dissociation process with this feature is reaction (6) which yields  $\text{O} + \text{HONO}$  both in their electronic ground states. Thus the photodissociation reactions (3), (4) and (6) all are forming oxygen and HONO but in different electronic states and consequently with different translational and rovibrational energy distributions. The average translational energy is  $\sim 4$  kJ/mol for (4),  $\sim 33$  kJ/mol for (3) and  $\sim 140$  kJ/mol for (6) with the corresponding widths of about 10, 50 and 80 kJ/mol, respectively. In reaction (4) most of the available energy  $E_{\text{avl}}$  is channeled into triplet excitation (252 kJ/mol) of HONO ( $\tilde{\text{a}}^3\text{A}''$ ), while in reaction (6) this energy is also available for the translational and internal energies of the fragments resulting in the broad  $E_{\text{T}}^{\text{total}}$  shown in Fig. 4b.

With regard to the previously unobserved reaction (6), a reinspection of the TOF spectra recorded at  $m/e = 16(\text{O}^+)$  and displayed as Fig. 3c in [9] turned out to be beneficial. A small signal between 50 and 100  $\mu\text{s}$  flight time, positioned just in front of the large signal from the oxygen fragments of reaction (3) and neglected in our previous

analyses, revealed after transformation to a  $E_{\text{T}}^{\text{total}}$  a similar distribution as that in Fig. 4b for reaction (6) which maximizes at 140 kJ/mol. Hence attributing the fast and small signal in Fig. 3c of [9] to reaction (6) and comparing its area to that of reaction (3) in the TOF spectrum, a ratio of roughly 1:10 is found. Since the quantum yield  $\phi(3) = 0.54$  [10] we obtain an estimated yield for reaction (6) of  $\approx 0.06$  which is even smaller than the indirect estimate given above. Though this value might be subject to a substantial error, the small quantum yield is certainly consistent with the spin-forbidden character of dissociation (6) and also supports our assumption that the amount of OH radicals from the secondary decay of hot HONO to  $\text{OH} + \text{NO}$  (which concerns about one third of the HONO products of (6)) is small and therefore introduces no serious errors when neglected in the rotational distribution analysis (Fig. 2).

To address the anisotropy of the five decay channels of  $\text{HNO}_3$  at 193 nm we find from previous measurements [9,10] the following parameters:  $\beta(1) = \beta(2) = -0.6$ ,  $\beta(3) = +0.6$  or 1.4; and  $\beta(4) = \beta(6) = +0.9$  from the present work. Channels (1) and (2) leading to  $\text{OH} + \text{NO}_2$  have a negative and, within experimental error, identical  $\beta$  value of  $-0.6$  whilst the three channels (3), (4) and (6) leading to  $\text{O} + \text{HONO}$  have positive values. Taking the uncertainty of  $\beta(3)$  into account which has been reported to be  $+0.6$  [9] and  $+1.4$  [10], it appears conceivable that the HONO channels also all possess similar  $\beta$  values around  $+1.0$ . The transition dipole moment  $\mu(\pi-\pi^*)$  at 193 nm lies in the molecular plane of  $\text{HNO}_3$ . Within  $C_{2v}$  symmetry, applicable if the OH group is treated as a pseudo-atom, the initially excited state has  $^1\text{B}_2$  symmetry and  $\mu$  is parallel to the line connecting the two terminal O atoms. This orientation is fully consistent with the  $\beta$  values of the two reaction types. For reaction type I including (1) and (2) the recoil direction is essentially perpendicular to  $\mu$  with  $\beta(1)$  and  $\beta(2)$  expected to be close to  $-1$  in the limit of prompt dissociation [28]. In reaction type II including (3), (4) and (6) however, the oxygen atom is expelled approximately along the direction of the breaking N–O bond implying a positive  $\beta$ , as observed. The calculated geometry of the excited state predicts an angle of about  $34^\circ$  between recoil

direction and  $\mu$  [29] from which a limiting value of  $\beta \sim 1.1$  is obtained. These anisotropy results are consistent with the two competing reaction types I and II each consisting of a branch of reactions which are all fast with respect to a rotational period of the parent molecule and involve no reaction steps which destroy the anisotropy.

### Acknowledgements

Support by the Schweizerischer Nationalfonds and by the Alfred Werner Legat is gratefully acknowledged. We thank PD Dr. P. Willmott for critically reading the manuscript.

### References

- [1] B.J. Finlayson-Pitts, J.N. Pitts, *Atmospheric Chemistry*, Wiley, New York, 1973.
- [2] R.P. Wayne, *Chemistry of Atmospheres*, Clarendon Press, Oxford, 1991.
- [3] A.A. Turnipseed, G.L. Vaghjiani, J.E. Thompson, A.R. Ravishankara, *J. Chem. Phys.* 96 (1992) 5887.
- [4] A. Schiffman, D.D. Nelson Jr., D.J. Nesbitt, *J. Chem. Phys.* 98 (1993) 6935.
- [5] J. August, M. Brouard, J.P. Simons, *J. Chem. Soc. Faraday Trans.* 84 (2) (1988) 587.
- [6] A. Sinha, R.L. Vander Wal, F.F. Crim, *J. Chem. Phys.* 91 (1989) 2929.
- [7] J. Schlütter, K. Kleinermanns, *Chem. Phys. Lett.* 192 (1992) 94.
- [8] S.J. Baek, C.R. Park, H.L. Kim, *J. Photochem. Photobiol. A* 104 (1997) 13.
- [9] P. Felder, X. Yang, J.R. Huber, *Chem. Phys. Lett.* 215 (1993) 221.
- [10] T.L. Myers, N.R. Forde, B. Hu, D.C. Kitchen, L.J. Butler, *J. Chem. Phys.* 107 (1997) 5361.
- [11] A. Jacobs, K. Kleinermanns, H. Kuge, J. Wolfrum, *J. Chem. Phys.* 79 (1983) 3162.
- [12] G.-H. Leu, C.-W. Hwang, I.-C. Chen, *Chem. Phys. Lett.* 257 (1996) 481.
- [13] O. Rattigan, E. Lutman, R.L. Jones, R.A. Cox, K. Clemitshaw, J. Williams, *J. Photochem. Photobiol. A* 66 (1992) 313.
- [14] JANAF Thermochemical Tables, *J. Phys. Chem. Ref. Data*, 14 (Suppl. 1) (1985).
- [15] E. Kades, M. Rösslein, U. Brühlmann, J.R. Huber, *J. Phys. Chem.* 97 (1993) 989.
- [16] E. Kades, M. Rösslein, J.R. Huber, *J. Phys. Chem.* 98 (1994) 13556.
- [17] M.-A. Thelen, P. Felder, J.R. Huber, *Chem. Phys. Lett.* 213 (1993) 275.
- [18] G.H. Dieke, H.M. Crosswhite, *J. Quant. Spectrosc. Radiat. Transfer* 2 (1962) 97.
- [19] I.L. Chidsey, D.R. Crosley, *J. Quant. Spectrosc. Radiat. Transfer* 23 (1980) 187.
- [20] C.J. Kreher, R.T. Carter, J.R. Huber, *J. Chem. Phys.* 110 (1999) 3309.
- [21] K. Bergmann, R.T. Carter, G.E. Hall, J.R. Huber, *J. Chem. Phys.* 109 (1998) 474.
- [22] C.E. Moore, *Atomic Energy Levels*, vol. 1 in Circular 467, National bureau of Standards, Washington, DC, 1949.
- [23] R.K. Sparks, K. Shobatake, L.R. Carlson, Y.T. Lee, *J. Chem. Phys.* 75 (1981) 3838.
- [24] J. Luque, D.R. Crosley, LIFBASE: Database and Spectral Simulation Program (Version 1.5), SRI International Report MP 99-009, 1999.
- [25] P. Andresen, G.S. Ondrey, B. Titze, E.W. Rothe, *J. Chem. Phys.* 80 (1984) 2548.
- [26] W. Schneider, G.K. Moortgat, G.S. Tyndall, J.P. Burrows, *J. Photochem. Photobiol. A* 40 (1987) 195.
- [27] C. Larrieu, A. Dargelos, M. Chaillet, *Chem. Phys. Lett.* 91 (1982) 465.
- [28] S. Yang, R. Bersohn, *J. Chem. Phys.* 61 (1974) 4400.
- [29] Y.Y. Bai, G.A. Segal, *J. Chem. Phys.* 92 (1990) 7479.